

A GLOBAL STAR FORMING EPISODE IN M31 2-4 GYR AGO

BENJAMIN F. WILLIAMS¹, JULIANNE J. DALCANTON¹, ANDREW E. DOLPHIN², DANIEL R. WEISZ^{1,4}, ALEXIA R. LEWIS¹,
DUSTIN LANG³, ERIC F. BELL⁵, MARTHA BOYER⁶, MORGAN FOUESNEAU⁷, KAROLINE M. GILBERT⁸, ANTONELA
MONACHESI⁹, EVAN SKILLMAN¹⁰

Draft version August 16, 2021

ABSTRACT

We have identified a major global enhancement of star formation in the inner M31 disk that occurred between 2-4 Gyr ago, producing $\sim 60\%$ of the stellar mass formed in the past 5 Gyr. The presence of this episode in the inner disk was discovered by modeling the optical resolved star color-magnitude diagrams of low extinction regions in the main disk of M31 ($3 < R < 20$ kpc) as part of the Panchromatic Hubble Andromeda Treasury. This measurement confirms and extends recent measurements of a widespread star formation enhancement of similar age in the outer disk, suggesting that this burst was both massive and global. Following the galaxy-wide burst, the star formation rate of M31 has significantly declined. We briefly discuss possible causes for these features of the M31 evolutionary history, including interactions with M32, M33 and/or a merger.

1. INTRODUCTION

Perhaps the only external massive galaxy for which we can hope to obtain detailed observational evolutionary constraints with the current generation of technology is the Local Group large spiral galaxy M31. Its mass ($1.4 \times 10^{12} M_{\odot}$; Watkins et al. 2010) and morphology (SA(s)b; de Vaucouleurs et al. 1991) are similar to those of the galaxies that dominate redshift surveys. Its nearby distance (770 kpc; McConnachie et al. 2005), low foreground extinction (A_V of 0.17 mag; Schlafly & Finkbeiner 2011), and relatively favorable inclination ($\sim 77^\circ$ not constant, Braun 1991) make it possible to study in great detail. All of these characteristics make M31 an excellent specimen to further our understanding of the formation and evolution of galaxies.

Even though M31 is so nearby, there are many challenges to unlocking its evolutionary history. First, its individual stars are not resolved from the ground beyond the top few magnitudes of the stellar luminosity function (Massey et al. 2006), and even these stars are often strongly affected by blending. Second, it is highly inclined and dusty (Dalcanton et al. 2015), complicating any interpretation of the stellar populations of the disk itself. Third, it is home to a massive bulge component

that dominates the stellar mass inside of ~ 1.5 kpc (e.g., Courteau et al. 2011; Dorman et al. 2013), further complicating interpretations of observational measurements. Fourth, the halo structure and satellite galaxy distribution are both complex, with the halo showing streams and multiple metallicity components (Ibata et al. 2001; Ferguson et al. 2002; McConnachie et al. 2009; Brown et al. 2003; Kalirai et al. 2006a,b; Gilbert et al. 2009, 2014; Ibata et al. 2014a) and the satellite population containing a co-planar set of dwarfs (Ibata et al. 2013).

Although the evolution of M31 has been somewhat difficult to determine, several resolved star studies have shown that the disk is dominated by stars older than 1 Gyr (Williams 2002; Bellazzini et al. 2003), and very deep resolved photometry of the outer disk suggests the disk is somewhat younger than the halo population (Brown et al. 2006). Further work on the outer disk has suggested a widespread (25–90 kpc deprojected radii) star formation episode at ~ 2 Gyr ago that may correspond to an encounter with M33 (Bernard et al. 2012, 2015), which also shows a peak in that age range (Williams et al. 2009). This idea is consistent with the many cold streams seen in the halo of M31, which are indicative of recent tidal interactions and many merger events (Ibata et al. 2001; Ferguson et al. 2002; McConnachie et al. 2009; Ibata et al. 2014b). In fact, the halo of M31 appears so much more complex than that of the Galaxy, that several have suggested that M31 could have undergone relatively recent (2-6 Gyr ago) mergers (Ibata et al. 2005; Hammer et al. 2010, 2013; Sadoun et al. 2014). Additionally, a relatively coeval population of massive star clusters was found by Fusi Pecci et al. (2005) with an age of ~ 2 Gyr, suggesting a significant star formation event at that time. Finally, very recent analysis of the kinematics of the M31 disk stars show that their velocity dispersion is significantly higher than that of the Galaxy, suggesting a more active merger history (Dorman et al. 2015).

In this paper, we make a new contribution to our understanding of the evolution of M31 by measuring the detailed age distribution of the stellar populations within the inner disk, showing how the burst seen in the outer galaxy persists to small galactic radii. By picking out the

¹ Department of Astronomy, Box 351580, University of Washington, Seattle, WA 98195; ben@astro.washington.edu, jd@astro.washington.edu, dweisz@astro.washington.edu

² Raytheon, 1151 E. Hermans Road, Tucson, AZ 85706; adolphin@raytheon.com

³ McWilliams Center for Cosmology, Department of Physics, Carnegie Mellon University, 5000 Forbes Ave., Pittsburgh, PA; dstn@cmu.edu

⁴ Hubble Fellow

⁵ Department of Astronomy, University of Michigan, 550 Church St., Ann Arbor MI 48109; ericbell@umich.edu

⁶ Observational Cosmology Lab, Code 665, NASA Goddard Space Flight Center, Greenbelt, MD 20771 USA; martha.boyer@nasa.gov

⁷ MPIA, Heidelberg; fousesneau@mpia-hd.mpg.de

⁸ STScI; kgilbert@stsci.edu

⁹ MPA, Garching; antonela@mpa-garching.mpg.de

¹⁰ Department of Astronomy, University of Minnesota, 116 Church St. SE, Minneapolis, MN 55455; skillman@astro.umn.edu

stellar photometry of the dust-free regions of the PHAT survey, we have been able to make reliable model fits to the optical color magnitude diagrams for 9 regions, ranging from 3 to 20 kpc from the galactic center (deprojected). The results show a globally-significant episode of star formation 2-4 Gyr ago, confirming and magnifying the significance of the result of Bernard et al. (2015). Section 2 briefly describes the data set used and our fitting techniques, which are both described in detail elsewhere in the literature. Section 3 gives the results of our measurements, focusing on the past 5 Gyr, and Section 4 discusses the possible interpretations of the results, including interaction and merger scenarios.

2. DATA

The data we have used for this project is a subset of the photometry from the Panchromatic Hubble Andromeda Treasury (PHAT; Dalcanton et al. 2012; Williams et al. 2014). These data include ultraviolet (UV) through near infrared (NIR) resolved stellar photometry, as well as a sample of artificial stars taken at a range of stellar densities. The artificial stars are sufficient to determine the uncertainties and completeness as a function of wavelength and stellar density (Williams et al. 2014).

2.1. Identifying Low-Extinction Regions

Historically it has been challenging to model the stellar populations of M31 inside of 20 kpc because of the high dust content which causes significant differential reddening (e.g. Dalcanton et al. 2012; Draine et al. 2014). To overcome this difficulty, we take advantage of the large contiguous area of the PHAT survey to find small regions containing very little extinction.

The photometry sample for our study was chosen using the extinction maps of Dalcanton et al. (2015), where dozens of $15'' \times 15''$ (60pc x 250pc, deprojected) dust-free regions were found across PHAT footprint by measuring the width of the red giant branch in the NIR. We selected 365 of these regions, and grouped them into 8 distinct areas to provide a wide range of radius and azimuth: five areas along the major axis, one along the minor axis, and three areas of large deprojected radius.

Figure 1 shows our groups plotted on both a map of the RGB width within the PHAT footprint as well as a 3.6 micron Spitzer map of M31. Table 1 provides the median, minimum, and maximum deprojected radii, total area, total number of stars, and best-fit differential reddening for each group. The group numbers in the table correspond to the labels on the figure.

2.2. Measuring Star Formation Histories

The color-magnitude diagrams of 6 of our 8 groups, which span the range of photometric quality of our data, are shown in Figure 2. While the red giant branch (RGB) of samples from smaller radii are broader due to crowding effects (see Williams et al. 2014, for details), these RGBs are narrow and well-defined. In addition, the red clump feature, visible at $F814W \sim 24.5$ in all CMDs sensitive to that depth, shows very little, if any, extension. These CMDs are consistent with the Dalcanton et al. (2015) measurement of these regions containing <0.6 mag of differential extinction. As a result, we allowed up to 0.6 mag of differential extinction (dA_V) in our model fits.

Including this small amount of differential extinction improved the fits, and did not change the measured age distributions beyond our measured uncertainties. However, it did impact some of the details of the star formation histories (SFHs) at intermediate ages in the 2 innermost groups. These groups were best-fit with $dA_V=0.4-0.6$ mag. The exact choice of dA_V had no effect on our result within our uncertainties. However, if no differential extinction was included at these radii, the results differed significantly, and were considerably less consistent with the results at larger radii.

We chose these regions because of their lack of dust. Therefore, they are biased against containing recent star formation. Thus, we have confined our comparison across the disk to ages >500 Myr. Ages younger than this are explored in detail in Lewis et al. (2014) and are highly structured spatially. By 500 Myr, the structure is still apparent, though less pronounced. In any case, this bias is unavoidable for our present analysis, so we will take it into consideration in any interpretations of our results.

Each of these groups has an appropriate set of artificial stars measured from a region of similar stellar density. To maximize our age sensitivity, we fit the optical CMDs of each set of photometry and artificial stars using the software package MATCH, using techniques well documented in the literature (Dolphin 2002; Gallart et al. 2005; Dolphin 2012, 2013; Weisz et al. 2014). In short, the CMD is binned into a 2-D histogram, and this histogram is fitted by a linear combination of model histograms from a fine grid of age and metallicity. The best-fit provides the most likely age and metallicity distribution for the stars. We then apply a Monte Carlo technique for determining the range of SFHs that would provide acceptable fits to the data. The results of the Monte Carlo runs yield random uncertainties for our measurements given the reliability of the models (Dolphin 2013).

To determine the significance of a particular feature in the best-fitting SFH, one must account for systematic uncertainties that come from deficiencies in the models or offsets between the models and measurements. The technique for determining these uncertainties is detailed in (Dolphin 2012). Briefly, the photometry is fitted to the models in 50 independent runs. In each run, the models are shifted with respect to the data by a random and small amount (± 0.02 in log of the effective temperature and ± 0.17 in bolometric magnitude). The results of the 50 runs are merged to calculate the variance of the results in each time bin, which is adopted as the systematic uncertainty. These uncertainties were combined with the random uncertainties to produce our total uncertainties on our age distributions.

We fit our data using several different stellar evolution models. We adopted fits with the Padova models (Girardi et al. 2000; Marigo et al. 2008) as our fiducial SFHs; however, we show the nominal SFHs using the BASTI (Pietrinferni et al. 2004) and PARSEC (Bressan et al. 2012) stellar evolution libraries to give a sense of the effects that different models have on age when fitting data of our varying depths.

We also produced model CMDs of constant star formation rate over the past 14 Gyr, convolved with the errors, completeness, and reddening measured from the PHAT data of varying depths. We fitted these using the same

techniques used to fit the observed CMDs. As with the extensive tests of such fitting in the literature (e.g. Dolphin 2002), in our tests, the measured SFHs fell within the uncertainties of the input constant SFH at the full range of photometric depths included in our data.

2.3. Comparisons with Deeper Photometry

In addition to our new measurements, we tested our ability to recover reliable SFHs using data of the depth and quality of the PHAT photometry. Our test data were taken from the HST archive using the ACS field in the warp in the outer regions of the southern M31 disk, previously analyzed in detail by Bernard et al. (2012). This field has very deep data and contains a clear feature at ~ 2 Gyr in the published age distribution. We analyzed this field in two ways. First, we ran the entire data set through our entire photometry and CMD-fitting technique with the Padova models to ensure that we could reproduce the Bernard et al. (2012) result. Then, we reduced a subset of the data to mimic the depth of the PHAT photometry in order to look for biases in the distribution of ages younger than 5 Gyr that could potentially be attributed to the shallower nature of the PHAT survey. Even using only a small subset of the Bernard et al. (2012) data resulted in relatively deep photometry due to the low stellar density of the far outer disk, so we limited the fitting to a portion of the CMD similar to the portion we were able to fit using the PHAT data in our inner fields (see black line in the upper-right panel of Figure 3). Thus, when fitting the shallow data, the fitting routine had no access to the subgiant branch or lower main-sequence, as these features fall outside of the included portion of the shallow CMD.

Figure 3 shows comparison between the age distributions younger than 5 Gyr from fitting the full depth of the data and from the much shallower subset of the data. We do not include ages greater than 5 Gyr on the plots to focus on the performance in the epoch of interest.¹¹ Thus the cumulative fractions are relative to only the subset of stars with ages < 5 Gyr, not the total stellar population. We outline the timing of the burst we find in the inner disk by shading different epochs. The age distribution from the full depth is shown with the dashed line. As published in Bernard et al. (2012) this SFH has a lull in star formation at 4-5 Gyr followed by a sharp burst at 2-3 Gyr. The fit to the shallower data also detects a burst at 2-3 Gyr, but ascribes $\sim 25\%$ more of the < 5 Gyr old stellar population to the burst than the fit to the deep data. Thus, both measurements agree on the presence of the burst, though its exact strength is more uncertain for the shallower data. However, the two measurements are fully consistent within the uncertainties, shown as the gray shaded region, confirming that our technique accurately estimates the precision with which we can determine the SFH in this age range.

3. RESULTS AND DISCUSSION

In Figure 4, we show the cumulative age distributions as a function of lookback time for six of our eight groups. As in Figure 3, we focus on the stars formed in the past

¹¹ The CMDs all contain a significant fraction of stars older than 5 Gyr, which were also measured by the SFH fitting. We leave the contribution of these stars out of the current analysis.

5 Gyr. The uncertainties for our adopted fits (those with the Padova models) are shown on the cumulative distributions as gray shaded areas. We also show the best fits from the BASTI and PARSEC models as dashed and dotted lines, respectively.

3.1. A Global Burst of Star Formation

Fits to all model sets show that the population of stars with ages < 5 Gyr is dominated by a strong episode of star formation. All of our SFHs show that star formation essentially shuts down over the past 1-2 Gyr, after undergoing a significant burst of star forming activity 2.0-3.5 Gyr ago. The possible exception is in the group near 7.8 kpc, where star formation was more steady.

Since our data are not of sufficient depth to probe the main sequence turnoff for stars of ages 2-3 Gyr, it is not necessarily instantly obvious which CMD feature is driving the detection of the large population of stars with these ages in our data. To qualitatively assess the detection, we produced model CMDs using the best fit and omitting the star formation from 2.0-3.5 Gyr, using the 4.7 kpc group as a fiducial. These model CMDs, along with the observed CMD and the difference between the two, are shown in Figure 5. The driving features appear to be the bright-blue portion of the red clump, the asymptotic giant branch, and the relatively blue and vertically oriented portion of the red giant branch. These features are apparently fit best by models of 2.0-3.5 Gyr in age. We have verified that models of older age with lower metallicity provide a poorer fit, as do models of constant star formation rate.

We note that these CMD features are not the most well-tested in the stellar evolution models (e.g. Gallart et al. 2005). Therefore, there is a chance that future changes to models of the red giant branch, asymptotic giant branch, and red clump models and/or deeper data could prove the population consistent with a more constant SFH. However, the detection of a burst of the same age in 14 deeper fields in the outer disk (25-90 kpc deprojected radii) at a variety of azimuthal angles (Bernard et al. 2015), along with the agreement between our fields of depths varying by 2 magnitudes and covering 17 kpc of the inner disk in deprojected galactocentric distance, strongly suggests that our result is robust given the models currently available for fitting resolved stellar photometry.

3.1.1. Age of the Burst

While the detection of a burst of star formation in M31 in the past 5 Gyr appears clear, it is difficult to pinpoint the age of the episode given the depth of our data. The age of the episode is most uncertain at the inner radii where the data are shallower, as shown by both the uncertainties and the very different ages measured from fits to different models. We note that if we could isolate the age more precisely than 1 Gyr, the burst could have been shorter and more intense; thus, the measured amplitude of the increase is a lower limit and the duration of ~ 1.5 Gyr is an upper limit. The model dependence of the age means that our precision on the burst age is limited to 2-4 Gyr ago (single digit precision) although our analysis with the Padova models alone would place the age at 2.0-3.5 Gyr.

3.1.2. Stellar Mass Produced

To investigate the amount of stellar mass formed in this burst, we calculated the surface density of the stellar mass formed from 2.0 to 3.5 Gyr ago as a function of median radius, and we compared this with the surface density of stars formed over other epochs of similar duration from 0.5-5.0 Gyr ago. These epochs are marked on Figure 4. We avoid the most recent 500 Myr as our regions were chosen to avoid dust, making us biased against recent star formation, and because this time period is investigated in detail in Lewis et al. (2014). We plot these profiles in the left panel of Figure 6. We note that the results from the shallower data at small radii are consistent with an extrapolation of the measurements from deeper data at larger radii. The right panel shows a sand-pile histogram of the fraction of the total 0.5-5 Gyr old stellar mass formed in each epoch.

Integrating the exponential profile plotted for the 2.0-3.5 Gyr time period shown in green in Figure 6 (see Table 2), assuming azimuthal symmetry, yields $8.1 \times 10^9 M_{\odot}$ of stars formed. Integrating the exponential profile for the 3.5-5.0 Gyr period yields only $2.5 \times 10^9 M_{\odot}$, and the profile for the 0.5-2.0 Gyr epoch also yields only $2.2 \times 10^9 M_{\odot}$. Thus, this was a galaxy-wide factor of ~ 3 -4 increase in the star formation rate averaged over 1.5 Gyr, resulting in the production of $6 \times 10^9 M_{\odot}$ of additional stellar mass. Assuming $\sim 30\%$ star formation efficiency, this mass would be associated with $2 \times 10^{10} M_{\odot}$ of baryonic matter.

This large amount of star formation likely significantly depleted the gas supply, resulting in the low SFR seen today. The current gas mass in M31 is $\sim 7 \times 10^9 M_{\odot}$ (Draine et al. 2014), and the star formation rate is $\sim 0.7 M_{\odot} \text{ yr}^{-1}$, yielding a depletion timescale of ~ 10 Gyr. However, the low SFR of M31 puts it into a transition zone between the blue and red bimodal color populations of large galaxy surveys (Mutch et al. 2011). Thus, this recent burst may mark an event in M31 history that triggered the current global transformation toward the red sequence. We consider whether this star formation 2.0-3.5 Gyr ago may signify an interaction or merger below.

4. CAUSE OF THE BURST

There are at least 3 possible scenarios that could induce such global star formation in M31. One possibility was suggested by Bernard et al. (2015): a tidal interaction with M33 during that epoch. Another possibility is a very strong interaction with M32, which stripped M32 into the dwarf elliptical that it is today. Finally, there is the possibility that a relatively major merger coalesced 2 Gyr ago into what is now M31. We now discuss each of these possibilities in turn.

4.1. Interaction with M33 or M32

It is possible that an interaction with another Local Group galaxy triggered the star formation episode in M31 2-4 Gyr ago. If so, based on previous studies, the most likely candidates are M33 and/or M32.

The timing of the burst at 2-3 Gyr ago is consistent with that seen in the outer M31 disk by Bernard et al. (2015) with deeper data over 14 fields spread all over the outer M31 disk. Simulations that reproduce the current velocities and positions of M31 and M33 suggest a close

passage 2-3 Gyr ago (McConnachie et al. 2009). Furthermore, a similar burst of similar age is seen in the star formation history of M33 (see SFHs in Williams et al. 2009). Numerical simulations do show that interactions can increase star formation rates by factors of 4-5 (e.g. Springel 2000), but such increases are only seen in simulations of very close interactions between galaxies of similar mass.

There are some characteristics of the M31-M33 system that make the M31-M33 interaction explanation for such a star formation episode less clear. First is the amount of mass in stars formed. Second is galaxy mass and morphology.

Our measurements suggest that this burst was widespread and produced a large amount of stellar mass in the massive galaxy M31. A fly-by of a galaxy $\sim 10\%$ of the mass of M31 may not be provide enough of a perturbation and may not include enough gas to explain this amount of increased star formation.

Furthermore, the masses and morphologies of the two galaxies do not seem consistent with a strong interaction between them. When smaller galaxies interact with larger galaxies, typically the morphology of the less massive galaxy is more affected than that of the more massive one (e.g., Mayer et al. 2001; Governato et al. 2004). M33 has a relatively undisturbed morphology, showing only a warped outer disk and a disk break beyond 8 kpc (Ferguson et al. 2007; Williams et al. 2009; McConnachie et al. 2009) despite being significantly less massive. M31 has a highly evolved morphology, as if it has been subjected to strong interactions, forming a large bulge and relatively quiescent disk. Therefore, the morphologies of the two galaxies (especially that of M33) are not those expected if they have recently been through a strong interaction.

Still, the simultaneous nature of the episodes seen in M31 and M33 suggest that there could have been an interaction, and the simulations of McConnachie et al. (2009) suggest that such an interaction occurred ~ 2 -3 Gyr ago. Perhaps future simulations will show that a major star formation episode can be triggered in a massive galaxy without causing major morphological changes to a low-mass galaxy. Perhaps such a burst could occur if the M31 disk was relatively gas-rich at the time and if the interaction had just the right impact parameter and orientation to induce some kind of resonance in the disk. Detailed hydrodynamic simulations of all possible interactions between the systems may be required to answer this question.

On the other hand, the M31-M32 system appears more consistent with having undergone a strong interaction a few Gyr ago. Block et al. (2006) simulate a collision between M31 and M32 ~ 200 Myr ago, which is more recent than our measurements probe, but suggests that the system has interacted strongly in the past. Morphologically, as a very compact dwarf elliptical very close to M31, M32 appears more likely to have been strongly influenced by an interaction with M31 in the recent past. Furthermore, there is a significant 2-5 Gyr old population in M32 which comprises 40% of its mass (Davidge & Jensen 2007; Monachesi et al. 2012). It is possible that M32 is the remnant of a galaxy that was once more massive and gas rich (Bekki et al. 2001). This relatively gas rich galaxy could have strongly interacted with M31 about 2 or 4 Gyr ago, triggering the burst in M31 as well

as the centrally-concentrated star formation in M32, generating the 2-5 Gyr old population in M32, and leaving M32 the compact dwarf elliptical galaxy we see today. On the other hand, M32 does not currently show kinematic or structural evidence of a strong tidal disturbance (Lauer et al. 1998; Howley et al. 2013)

There is also the possibility that both of these scenarios occurred during the epoch in question. Perhaps M33 was much closer to M31 during this epoch (as in the simulations of McConnachie et al. 2009), explaining the increase SFR in M33 at that time. Furthermore, M32 could have been in the process of being stripped and both events could have contributed to the elevated star formation in M31.

4.2. Possible Merger

Another possible explanation for the episode is a merger with galaxy $\gtrsim 20\%$ of the pre-merger mass of M31, such as in the merger simulations of Cox et al. (2008). The density profile of the stars formed, the recent decrease in the M31 star formation rate, and the stellar mass produced are all consistent with a relatively large merger scenario, as described below.

Like the Cox et al. (2008) simulations, the density profile of the enhancement is similar in shape to the overall surface density profile of M31, as shown in Figure 6. Furthermore, the simulations show a smooth decrease in global star formation rate down to levels $\lesssim 1 M_{\odot} \text{ yr}^{-1}$ in the 2 Gyr following the merger as a result of gas depletion. Such a decrease is consistent with that recently measured by Lewis et al. (2014). The stellar density in the outer regions of merger simulations (e.g., Cox et al. 2008; Moreno et al. 2015) ~ 3 Gyr after the merger show only relatively faint structures, qualitatively similar to those observed in the M31 halo (Ibata et al. 2001; Ferguson et al. 2002; McConnachie et al. 2009).

The amount of stellar mass produced by the event hints at a relatively large merger. If the matter that formed the stars in the burst came from the galaxy that merged, the baryonic Tully-Fisher relation (Zaritsky et al. 2014, e.g.) yields a circular velocity of $\sim 140 \text{ km s}^{-1}$ for $2 \times 10^{10} M_{\odot}$ of baryonic mass, which is similar to the circular velocity of M33 (Corbelli & Salucci 2000). As some of the mass was in M31 already, this estimate is an approximate upper-limit on any infalling galaxy.

It is difficult to compare our SFHs of relatively low time resolution to the SFHs of the Cox et al. (2008) simulations directly. However, a 1:1 merger ratio in their simulations appears to produce more than the equivalent of a factor of 2 increase in star formation rate for 1.5 Gyr. Such an equal-mass merger appears to produce the equivalent of about a factor of $\gtrsim 10$ increase for 1 Gyr. The 5.8:1 merger does not appear to enhance the star formation enough to produce the effect we see in the M31

data. The mean rate increase of a factor of 4-5 over about a Gyr we see in our data is limited by our time resolution. The actual burst could have had a much shorter duration, but produced enough stellar mass for us to detect it throughout the galaxy. Most consistent with merger simulations would be another galaxy $\gtrsim 20\%$ of the pre-merger mass of M31. Such a total mass ($\sim 2 \times 10^{11} M_{\odot}$) is reasonable considering the baryonic mass estimate above of $\sim 2 \times 10^{10} M_{\odot}$.

The merger scenario also has problems. First, it is unclear if the M31 disk would have survived, even in its relatively quiescent state, if it had undergone such a merger. However, simulations do suggest that disks can survive large mergers if they contain high gas fractions (Hopkins et al. 2009). Second, it is puzzling why M33 would show a simultaneous global star formation episode. However, it is possible that the galaxy that merged with M31 passed by M33 (which may have been much closer to M31 at the time McConnachie et al. 2009) along the way, inducing star formation during the same epoch but not strongly disturbing its morphology. Finally, very recent simulations by Moreno et al. (2015) suggest that most of the star formation in mergers occurs $< 1 \text{ kpc}$ from the galaxy center, which would not be consistent with this disk-wide burst in M31.

Whatever the explanation, these newly-measured age distributions from the PHAT survey provide a new piece of evidence, along with the structured halo (Hammer et al. 2010, 2013; Sadoun et al. 2014), structured satellite distribution (Ibata et al. 2013, 2014a), peak in massive cluster ages (Fusi Pecci et al. 2005), and velocity dispersion of the disk (Dorman et al. 2015) that point to M31 having undergone a significant interaction event in the past few Gyr.

In conclusion, we have found new evidence that a global burst of star formation occurred in M31 2-4 Gyr ago over the entire M31 disk. The cause of this burst is far from clear. It could have been due to interactions with M32 and/or M33. It could have been a merger, or it could be some combination of these. The occurrence of the burst may help to explain the current, low-activity state of the M31 disk and its current global transformation toward the red sequence. Future simulations may be able to provide more detailed constraints on the physical cause of the burst.

Support for this work was provided by NASA through grant GO-12055 from the Space Telescope Science Institute, which is operated by the Association of Universities for Research in Astronomy, Incorporated, under NASA contract NAS5-26555. Support for DRW is provided by NASA through Hubble Fellowship grants HST-HF-51331.01 awarded by the Space Telescope Science Institute. We thank Amazon cloud services, for donating some of the computing time necessary to make these measurements.

REFERENCES

- Bekki, K., Couch, W. J., Drinkwater, M. J., & Gregg, M. D. 2001, *ApJ*, 557, L39
 Bellazzini, M., Cacciari, C., Federici, L., Fusi Pecci, F., & Rich, M. 2003, *A&A*, 405, 867
 Bernard, E. J., et al. 2012, *MNRAS*, 420, 2625
 Bernard, E. J., et al. 2015, *MNRAS*, 446, 2789
 Block, D. L., et al. 2006, *Nature*, 443, 832
 Braun, R. 1991, *ApJ*, 372, 54
 Bressan, A., Marigo, P., Girardi, L., Salasnich, B., Dal Cero, C., Rubele, S., & Nanni, A. 2012, *MNRAS*, 427, 127

- Brown, T. M., Ferguson, H. C., Smith, E., Kimble, R. A., Sweigart, A. V., Renzini, A., Rich, R. M., & VandenBerg, D. A. 2003, *ApJ*, 592, L17
- Brown, T. M., Smith, E., Ferguson, H. C., Rich, R. M., Guhathakurta, P., Renzini, A., Sweigart, A. V., & Kimble, R. A. 2006, *ApJ*, 652, 323
- Corbelli, E., & Salucci, P. 2000, *MNRAS*, 311, 441
- Courteau, S., Widrow, L. M., McDonald, M., Guhathakurta, P., Gilbert, K. M., Zhu, Y., Beaton, R. L., & Majewski, S. R. 2011, *ApJ*, 739, 20
- Cox, T. J., Jonsson, P., Somerville, R. S., Primack, J. R., & Dekel, A. 2008, *MNRAS*, 384, 386
- Dalcanton, J. J., et al. 2015, *ApJ*, submitted
- Dalcanton, J. J., et al. 2012, *ApJS*, 200, 18
- Davidge, T. J., & Jensen, J. B. 2007, *AJ*, 133, 576
- de Vaucouleurs, G., de Vaucouleurs, A., Corwin, H. G., Jr., Buta, R. J., Paturel, G., & Fouqué, P. 1991, *Third Reference Catalogue of Bright Galaxies. Volume I: Explanations and references. Volume II: Data for galaxies between 0^h and 12^h. Volume III: Data for galaxies between 12^h and 24^h.*
- Dolphin, A. E. 2002, *MNRAS*, 332, 91
- Dolphin, A. E. 2012, *ApJ*, 751, 60
- Dolphin, A. E. 2013, *ApJ*, 775, 76
- Dorman, C., Guhathakurta, P., Seth, A., Dalcanton, J., Widrow, L., & Splash Team, P. T. 2015, in *American Astronomical Society Meeting Abstracts*, Vol. 225, American Astronomical Society Meeting Abstracts, 429.01
- Dorman, C. E., et al. 2013, *ApJ*, 779, 103
- Draine, B. T., et al. 2014, *ApJ*, 780, 172
- Ferguson, A., Irwin, M., Chapman, S., Ibata, R., Lewis, G., & Tanvir, N. 2007, *Resolving the Stellar Outskirts of M31 and M33 (Island Universes - Structure and Evolution of Disk Galaxies)*, 239
- Ferguson, A. M. N., Irwin, M. J., Ibata, R. A., Lewis, G. F., & Tanvir, N. R. 2002, *AJ*, 124, 1452
- Fusi Pecci, F., Bellazzini, M., Buzzoni, A., De Simone, E., Federici, L., & Galletti, S. 2005, *AJ*, 130, 554
- Gallart, C., Zoccali, M., & Aparicio, A. 2005, *ARA&A*, 43, 387
- Gilbert, K. M., Font, A. S., Johnston, K. V., & Guhathakurta, P. 2009, *ApJ*, 701, 776
- Gilbert, K. M., et al. 2014, *ApJ*, 796, 76
- Girardi, L., Bressan, A., Bertelli, G., & Chiosi, C. 2000, *A&AS*, 141, 371
- Governato, F., et al. 2004, *ApJ*, 607, 688
- Hammer, F., Yang, Y., Fouquet, S., Pawlowski, M. S., Kroupa, P., Puech, M., Flores, H., & Wang, J. 2013, *MNRAS*, 431, 3543
- Hammer, F., Yang, Y. B., Wang, J. L., Puech, M., Flores, H., & Fouquet, S. 2010, *ApJ*, 725, 542
- Hopkins, P. F., Cox, T. J., Younger, J. D., & Hernquist, L. 2009, *ApJ*, 691, 1168
- Howley, K. M., et al. 2013, *ApJ*, 765, 65
- Ibata, R., Chapman, S., Ferguson, A. M. N., Lewis, G., Irwin, M., & Tanvir, N. 2005, *ApJ*, 634, 287
- Ibata, R., Irwin, M., Lewis, G., Ferguson, A. M. N., & Tanvir, N. 2001, *Nature*, 412, 49
- Ibata, R. A., Ibata, N. G., Lewis, G. F., Martin, N. F., Conn, A., Elahi, P., Arias, V., & Fernando, N. 2014a, *ApJ*, 784, L6
- Ibata, R. A., et al. 2013, *Nature*, 493, 62
- Ibata, R. A., et al. 2014b, *ApJ*, 780, 128
- Kalirai, J. S., et al. 2006a, *ApJ*, 648, 389
- Kalirai, J. S., Guhathakurta, P., Gilbert, K. M., Reitzel, D. B., Majewski, S. R., Rich, R. M., & Cooper, M. C. 2006b, *ApJ*, 641, 268
- Lauer, T. R., Faber, S. M., Ajhar, E. A., Grillmair, C. J., & Scowen, P. A. 1998, *AJ*, 116, 2263
- Lewis, A., et al. 2014, *ApJ*, submitted
- Marigo, P., Girardi, L., Bressan, A., Groenewegen, M. A. T., Silva, L., & Granato, G. L. 2008, *A&A*, 482, 883
- Massey, P., Olsen, K. A. G., Hodge, P. W., Strong, S. B., Jacoby, G. H., Schlingman, W., & Smith, R. C. 2006, *AJ*, 131, 2478
- Mayer, L., Governato, F., Colpi, M., Moore, B., Quinn, T., Wadsley, J., Stadel, J., & Lake, G. 2001, *ApJ*, 559, 754
- McConnachie, A. W., Irwin, M. J., Ferguson, A. M. N., Ibata, R. A., Lewis, G. F., & Tanvir, N. 2005, *MNRAS*, 356, 979
- McConnachie, A. W., et al. 2009, *Nature*, 461, 66
- Monachesi, A., Trager, S. C., Lauer, T. R., Hidalgo, S. L., Freedman, W., Dressler, A., Grillmair, C., & Mighell, K. J. 2012, *ApJ*, 745, 97
- Moreno, J., Torrey, P., Ellison, S. L., Patton, D. R., Bluck, A. F. L., Bansal, G., & Hernquist, L. 2015, *ArXiv e-prints*
- Mutch, S. J., Croton, D. J., & Poole, G. B. 2011, *ApJ*, 736, 84
- Pietrinferni, A., Cassisi, S., Salaris, M., & Castelli, F. 2004, *ApJ*, 612, 168
- Sadoun, R., Mohayaee, R., & Colin, J. 2014, *MNRAS*, 442, 160
- Schlafly, E. F., & Finkbeiner, D. P. 2011, *ApJ*, 737, 103
- Springel, V. 2000, *MNRAS*, 312, 859
- Watkins, L. L., Evans, N. W., & An, J. H. 2010, *MNRAS*, 406, 264
- Weisz, D. R., Dolphin, A. E., Skillman, E. D., Holtzman, J., Gilbert, K. M., Dalcanton, J. J., & Williams, B. F. 2014, *ApJ*, 789, 147
- Williams, B. F. 2002, *MNRAS*, 331, 293
- Williams, B. F., Dalcanton, J. J., Dolphin, A. E., Holtzman, J., & Sarajedini, A. 2009, *ApJ*, 695, L15
- Williams, B. F., et al. 2014, *ArXiv e-prints*
- Zaritsky, D., et al. 2014, *AJ*, 147, 134

TABLE 1
PROPERTIES OF THE 9 SAMPLES TAKEN FROM THE PHAT DUST-FREE REGIONS

Region	R_{deproj} (kpc)	Min_{deproj} (kpc)	Max_{deproj} (kpc)	Area (kpc ²)	N_{stars}	Σ (arcsec ⁻²)	dA_V (mag)
1	3.00	2.69	3.46	0.075	122561	22.7	0.4
2	4.69	4.13	4.93	0.034	50177	20.3	0.6
3	7.81	7.19	8.51	0.182	198732	15.2	0.4
4	14.24	13.42	14.92	0.075	47038	8.7	0.2
5	16.94	15.32	19.35	0.245	131251	7.5	0.2
6	17.67	17.17	18.52	0.044	15078	4.8	0.0
7	18.34	17.19	19.87	0.288	91090	4.3	0.0
8	18.81	17.15	19.93	0.191	48055	3.5	0.2

TABLE 2
EXPONENTIAL PROFILE FIT PARAMETERS AND INTEGRATED STELLAR MASSES FOR THE THREE AGE RANGES

Age Range	Scale Length (kpc)	Normalization (M_{\odot} kpc ⁻²)	Integrated Stellar Mass (M_{\odot})
0.5-2.0 Gyr	7.1±1.0	8.9±3.7×10 ⁶	2.2±1.1×10 ⁹
2.0-3.5 Gyr	4.5±0.5	6.6±2.1×10 ⁷	8.0±2.5×10 ⁹
3.5-5.0 Gyr	4.9±0.8	1.8±1.0×10 ⁷	2.5±1.1×10 ⁹

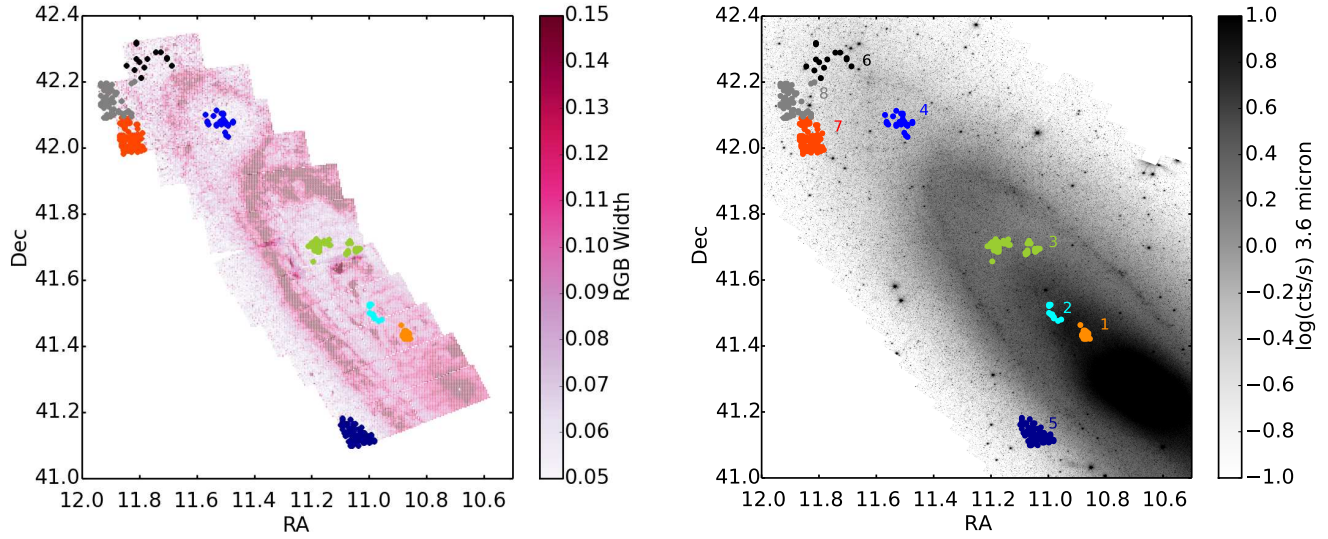


FIG. 1.— *Left:* Locations in the PHAT footprint of our “reddening-free” samples are overplotted on a map of the width of the red giant branch as measured in the NIR photometry. This width is a proxy for the amount of dust present along the line of sight. The sample comes from the regions of narrowest width, and therefore containing very little dust. Circles of the same color show how we grouped the samples to improve our CMD-fitting statistics. *Right:* Locations in the PHAT footprint of our “reddening-free” samples are overplotted on a *Spitzer* 3.6 μ image, showing the wide range of stellar densities covered by our samples. However, groups are confined to areas with little stellar density variation. Numbers label each group with their region number in Table 1.

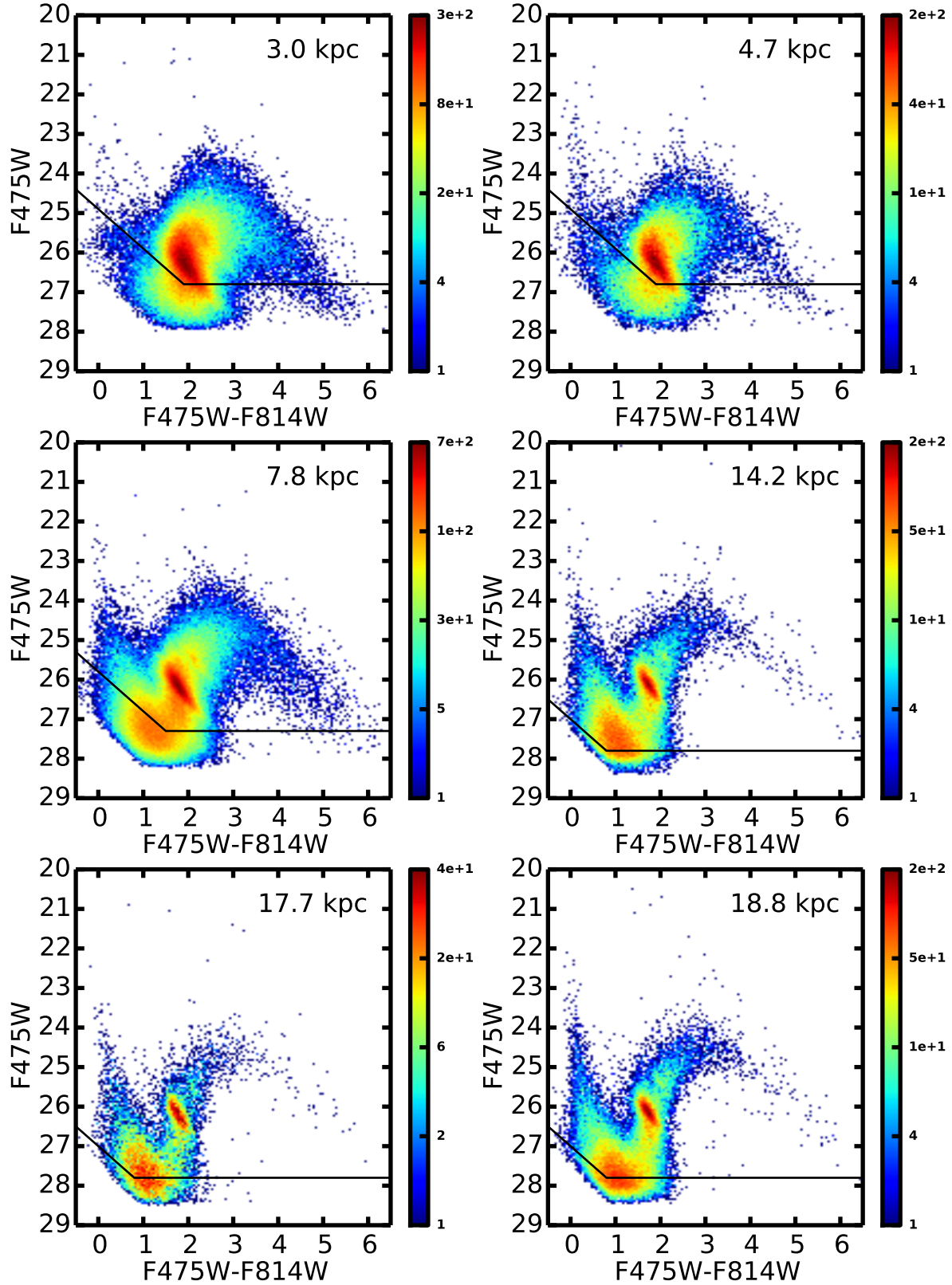


FIG. 2.— The color-magnitude diagrams of 6 of our sample groups at different radii along the major axis. Other regions are not shown for brevity. Color gives the number of stars per 0.05×0.05 mag CMD bin. All data above the black line was included in the fitting. All show well-behaved red giant branches, with no indication of differential reddening of more than ~ 0.5 mag. Crowding significantly limits photometric precision and depth inside of 5 kpc.

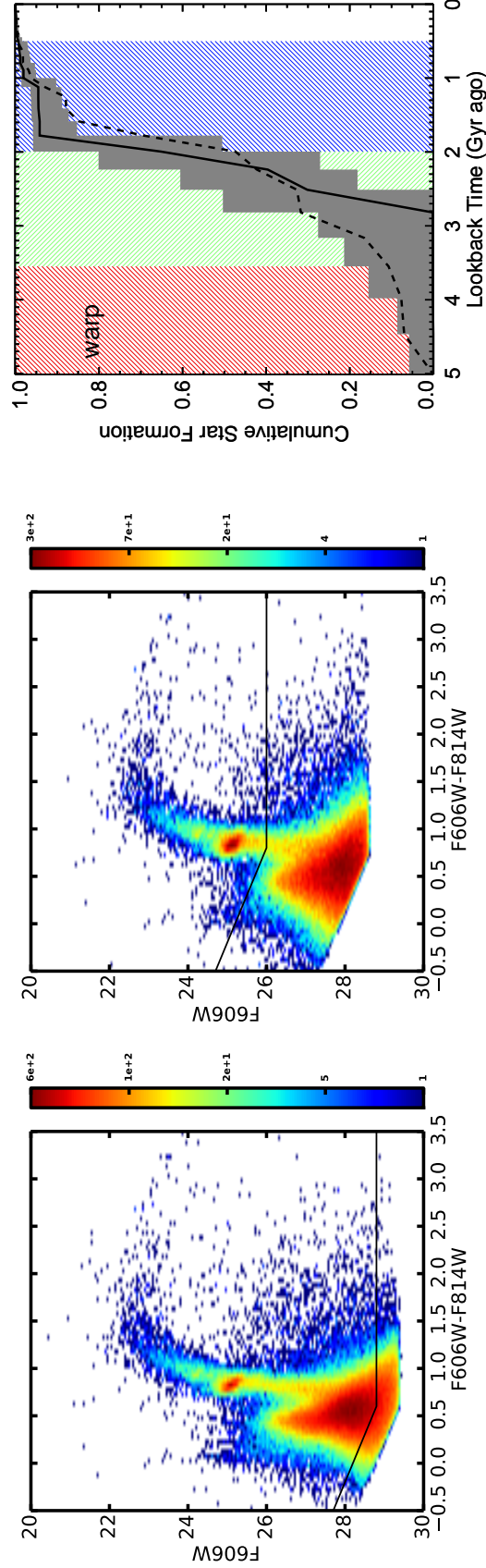


FIG. 3.— Testing the effects of depth on the recovered star age distribution over the past 5 Gyr. Although the CMDs all contain a significant fraction of stars older than 5 Gyr which were also measured by the SFH fitting, we leave the contribution from these stars out of the current analysis to focus on the epoch of interest. Thus all of the cumulative fractions are relative to only the subset of stars with ages < 5 Gyr, not the total stellar population. *Upper Left:* Color-magnitude diagram of our photometry from the warp field of Bernard et al. (2012), using their full set of HST exposures. We included all of the CMD above the black line in the fitting. *Upper Right:* Same as left, but from photometry performed using only 2 exposures in each band, of similar depth to the PHAT data. We included all of the CMD above the black line in the fitting. *Lower Left:* The cumulative star formation history of the warp field from Bernard et al. (2012). Three colored stripes show the 3 epochs used to make the plots in Figure 6, in their respective colors. The dashed line shows the best fit to the full-depth data, which is similar to their measurements. The solid line shows the best fit to the shallow photometry, and the dark gray shaded area shows the absolute uncertainties associated with the fit to the shallow photometry. Both measurements clearly detect the burst at ~ 2 Gyr, showing that even though the precision of the measurement from the shallow data is much worse, the absolute uncertainties are robust. *Lower Right:* The differential SFH of both fits. The thin black histogram shows the best-fit SFH to the full-depth data with associated uncertainties, and the thick gray histogram shows the best-fit SFH to the shallow data with associated uncertainties. Again, both measure a burst at ~ 2 Gyr, although the shallower data finds a slightly older and less precise age than the full-depth data.

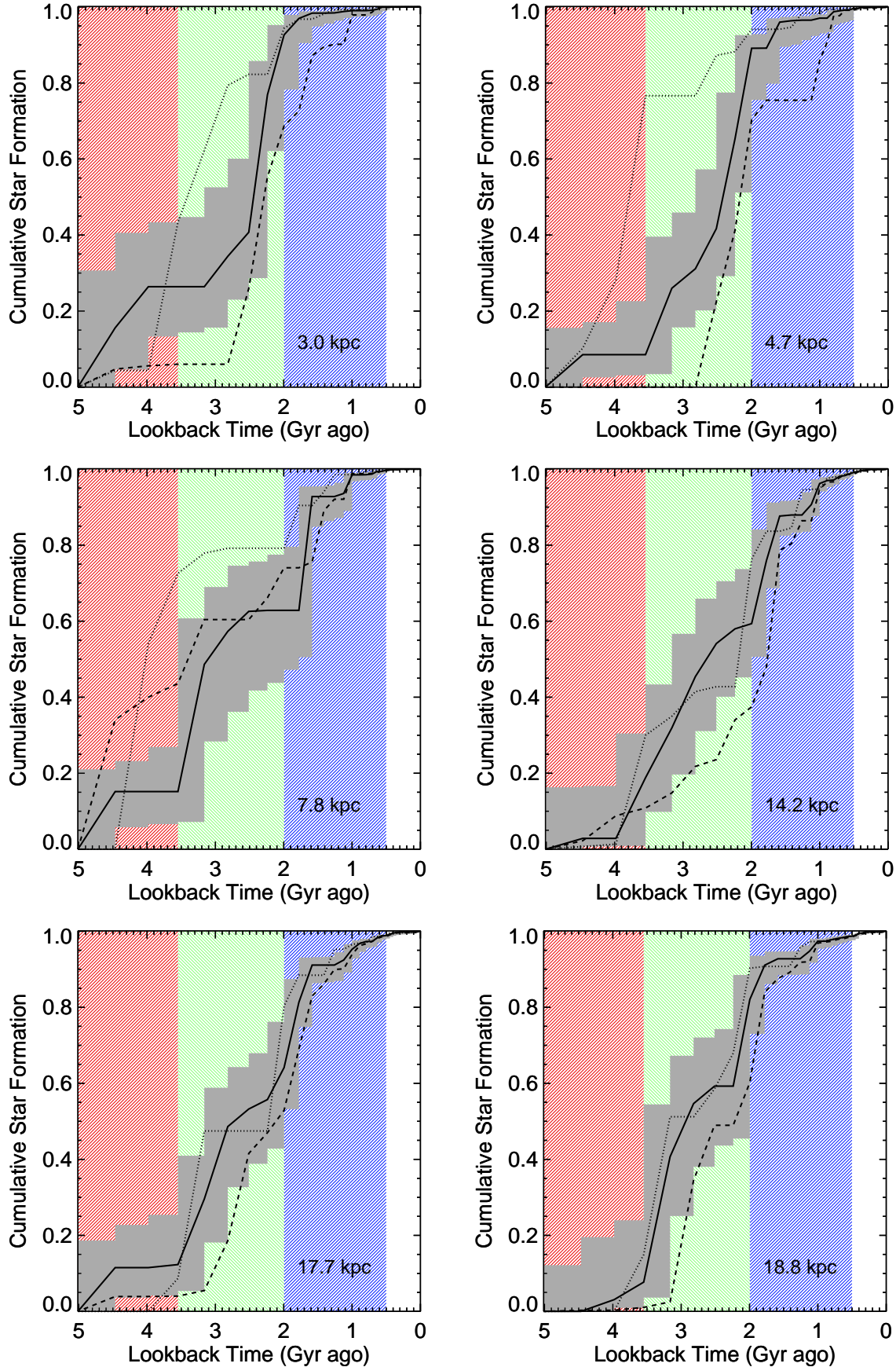


FIG. 4.— The cumulative star formation for the past 5 Gyr at 6 different radii. Other regions are not shown for brevity. These correspond to the six radial groupings along the major axis shown in Figure 1. Solid lines with gray shading show the fits to the Padova models along with the total uncertainties described in Section 2.1. Dashed lines show the best fit to the BASTI models, and dotted lines show the best fit to the PARSEC models. Three colored stripes show the 3 epochs used to make the plots in Figure 6, in their respective colors. All of the model sets result in a steep increase of short duration in all locations. The Padova models measure the burst to be 2.0-3.5 Gyr ago (green area of the plots) relative to the neighboring epochs. As in Figure 3, the cumulative fractions refer only to those stars formed in the last 5 Gyr.

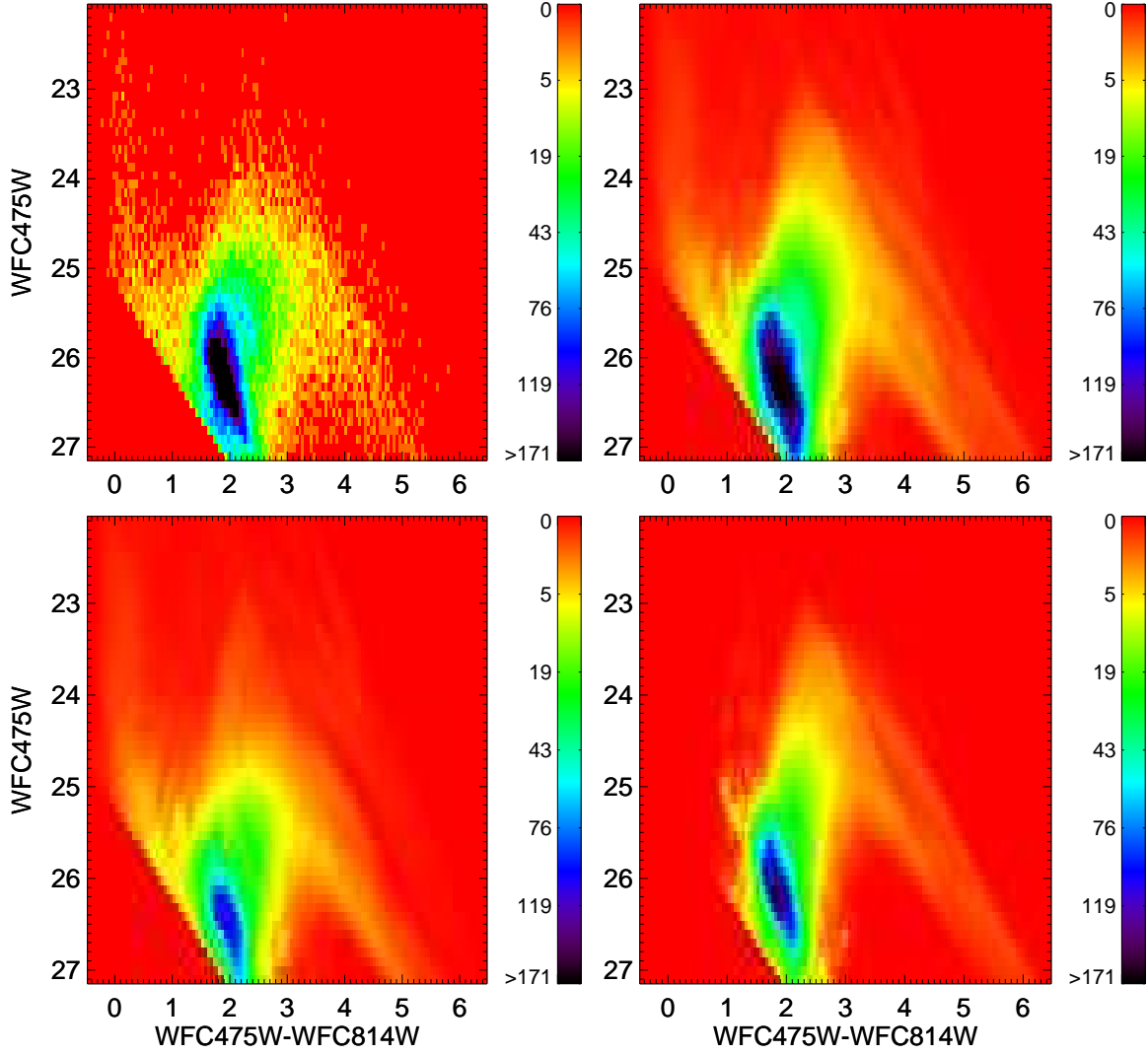


FIG. 5.— *Upper Left:* Observed CMD for the 4.7 kpc group. *Upper Right:* Best-fit Padova model CMD. *Lower Left:* Best-fit Padova model excluding all stars with ages from 2.0 to 3.5 Gyr. *Lower Right:* Difference between *upper right* and *lower left*, isolating the CMD features that indicate the presence of the enhancement at 2.0-3.5 Gyr.

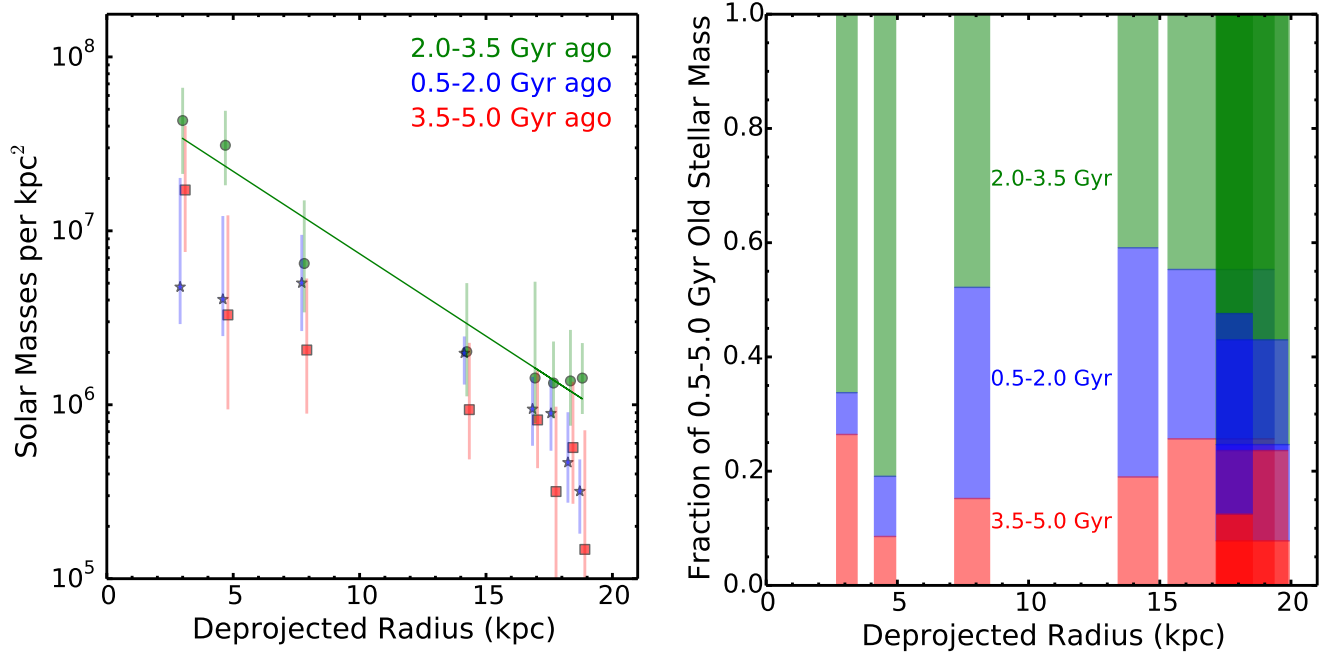


FIG. 6.— *Left:* Radial profiles of the stellar mass surface density of M31 in three age bins (see Table 2). Colors and symbol types represent the stellar mass contribution of several epochs of similar duration, shown as colored vertical stripes in Figure 4. The 2.0-3.5 Gyr old population (green/circles) dominates the stellar surface density. The best-fit exponential to this population is overplotted with the green line ($6.6 \times 10^7 e^{-r/4.6 \text{ kpc}}$). *Right:* Sand-pile histogram of the fraction of the 0.5-5.0 Gyr old population in each epoch is plotted as a function of deprojected radius.